ISSN 1063-7761, Journal of Experimental and Theoretical Physics, 2013, Vol. 116, No. 5, pp. 800–805. © Pleiades Publishing, Inc., 2013.
Original Russian Text © A.A. Demidov, D.V. Volkov, I.A. Gudim, E.V. Eremein, V.L. Temerov, 2013, published in Zhurnal Eksperimental'noi i Teoreticheskoi Fiziki, 2013, Vol. 143, No. 5, pp. 922–928.

ORDER, DISORDER, AND PHASE TRANSITION IN CONDENSED SYSTEM

Magnetic Properties of the Rare-Earth Ferroborate $SmFe_3(BO_3)_4$[1]

A. A. Demidov[a,*], D. V. Volkov[b], I. A. Gudim[c], E. V. Eremein[c], and V. L. Temerov[c]

[a] *Bryansk State Technical University, Bryansk, 241035 Russia*
**e-mail: demandr@yandex.ru*
[b] *Moscow State University, Moscow, 119992 Russia*
[c] *Kirensky Institute of Physics, Siberian Branch, Russian Academy of Sciences, Krasnoyarsk, 660036 Russia*

Abstract—The magnetic properties of trigonal antiferromagnet $SmFe_3(BO_3)_4$ are studied experimentally and theoretically. The measured characteristics are considered in terms of a theoretical approach based on the molecular field approximation and a crystal field model for a rare-earth ion. The temperature dependences of the initial magnetic susceptibility and the field and temperature dependences of magnetization in fields up to 5 T are described, and the anomaly in the magnetization curve for $\mathbf{B} \perp \mathbf{c}$ near 1 T, which points to a first-order phase transition, is analyzed.

DOI: 10.1134/S1063776113050038

1. INTRODUCTION

Interest in trigonal rare-earth ferroborates $RFe_3(BO_3)_4$ (R = Y, La–Lu) has recently been quickened because of the discovery of multiferroelectric properties in them [1, 2]. As compounds with two interacting magnetic (rare-earth, iron) subsystems, ferroborates are of particular interest for the physics of magnetic phenomena. The iron subsystem in $RFe_3(BO_3)_4$ is ordered at $T_N \approx 30$–40 K, and the rare-earth subsystem is magnetized by the *f–d* interaction and significantly contributes to the magnetic anisotropy and the orientation of magnetic moments. Ferroborates can be easy-axis and easy-plane ones and can spontaneously transform from an easy-axis into an easy-plane state (as in $GdFe_3(BO_3)_4$ and $HoFe_3(BO_3)_4$; see, e.g., review [3]).

In particular, keen interest in $SmFe_3(BO_3)_4$ is caused by the giant magnetodielectric effect revealed in it [4]. The entire information on the spectroscopic [5], magnetic, magnetoelectric, and magnetoelastic properties [3, 4, 6–8] indicates that the magnetic moments of iron in $SmFe_3(BO_3)_4$ are antiferromagnetically ordered at $T_N \approx 32$–33 K and lie in basal plane *ab*. The magnetic moments of samarium magnetized by the exchange field of iron also lie in the basal plane.

The purpose of this work is to study the low-temperature magnetic properties of $SmFe_3(BO_3)_4$ experimentally and theoretically, to compare the obtained experimental and calculated results, and to determine the compound parameters.

[1] The article is based on a preliminary report delivered at the 36th Conference on Low-Temperature Physics (St. Petersburg, July 2–6, 2012).

2. EXPERIMENTAL

The single crystals were grown from molten solutions based on bismuth trimolybdate 80 wt % $\{Bi_2Mo_3O_{12} + 2B_2O_3 + 0.6Sm_2O_3\}$ + 20 wt % $SmFe_3(BO_3)_4$ according to the process described in detail in [9]. The crystals were grown in a 150-g molten solution simultaneously on four seeds 1 mm^3 in size under the same hydrodynamic conditions. The supercooling corresponded to a growth rate of at most 1 mm/day. The samarium content in the crystals was determined by X-ray fluorescence analysis. Magnetic measurements were carried out on a Physical Properties Measurement System (Quantum Design) device in the temperature range 2–300 K at magnetic fields up to 5 T.

3. CALCULATION PROCEDURE

The magnetic properties of $SmFe_3(BO_3)_4$ are induced by both magnetic subsystems, namely, the rare-earth (samarium) and iron subsystems, interacting with each other. The interaction inside the Sm subsystem may be neglected. The iron subsystem can be considered as a set of two antiferromagnetic sublattices. The Sm subsystem magnetized by the *f–d* interaction can also be represented by two sublattices. In our calculations, we used the theoretical approach successfully applied to ferroborates $RFe_3(BO_3)_4$ with R = Tb [10], Nd [11], Dy [12], Pr [13], Ho [14], and Er [15]. For the magnetic structure and the hierarchy of interactions in $SmFe_3(BO_3)_4$ in magnetic field **B**, the effective Hamiltonians of a Sm/Fe ion in the *i*th ($i = 1, 2$) sublattice can be written as

$$\mathcal{H}_i(\mathrm{Sm}) = \mathcal{H}_i^{\mathrm{CF}} - g_J^{\mathrm{Sm}} \mu_B \mathbf{J}_i^{\mathrm{Sm}} [\mathbf{B} + \lambda_{\mathrm{fd}}^{\mathrm{Sm}} \mathbf{M}_i^{\mathrm{Fe}}], \quad (1)$$

$$\mathcal{H}_i(\mathrm{Fe}) = -g_S\mu_B\mathbf{S}_i[\mathbf{B} + \lambda\mathbf{M}_j^{\mathrm{Fe}} + \lambda_{\mathrm{fd}}^{\mathrm{Sm}}\mathbf{m}_i^{\mathrm{Sm}}], \quad j = 1, 2, \quad j \neq i, \tag{2}$$

where $\mathcal{H}_i^{\mathrm{CF}}$ is the crystal field Hamiltonian, g_J^{Sm} is the Landé factor; $\mathbf{J}_i^{\mathrm{Sm}}$ is the operator of the angular moment of the Sm ion; $g_S = 2$ is the g factor; $\mathbf{S}_i$ is the operator of the spin moment of the Fe ion; and $\lambda_{\mathrm{fd}}^{\mathrm{Sm}} < 0$ and $\lambda < 0$ are the molecular constants of the antiferromagnetic Sm–Fe and Fe–Fe interactions, respectively. The magnetic moments of the ith iron ($\mathbf{M}_i^{\mathrm{Fe}}$) and samarium ($\mathbf{m}_i^{\mathrm{Sm}}$) sublattices per formula unit are determined from the relationships

$$\mathbf{M}_i^{\mathrm{Fe}} = 3g_S\mu_B\langle\mathbf{S}_i\rangle, \quad \mathbf{m}_i^{\mathrm{Sm}} = g_J^{\mathrm{Sm}}\mu_B\langle\mathbf{J}_i^{\mathrm{Sm}}\rangle. \tag{3}$$

The Fe^{3+} ion in $RFe_3(BO_3)_4$ is in a high-spin state [16], which gives the maximum magnetic moment of the ion ($5\mu_B$).

It is known (see, e.g., [17, 18]) that the Hamiltonian of the trigonal symmetry crystal field of the Sm^{3+} ion ($J^{\mathrm{Sm}} = 5/2$) contains only three terms. In terms of irreducible tensor operators C_q^k, it has the form

$$\mathcal{H}^{CF} = B_0^2C_0^2 + B_0^4C_0^4 + B_3^4(C_{-3}^4 - C_3^4). \tag{4}$$

Crystal field parameters B_q^k for the Sm^{3+} ion in $SmFe_3(BO_3)_4$ are unknown. It is known from the spectroscopic investigations [5] that the splitting of the ground doublet of the Sm^{3+} ion in $SmFe_3(BO_3)_4$ at $T = 1.7$ K is $\Delta_{\mathrm{fd}} = 13.2$ cm^{-1} and that the lower part of the multiplet of the Sm^{3+} ion in the paramagnetic state is characterized by energies of 0, 135, and 220 cm^{-1}.

We calculated the values and orientations of the magnetic moments of the Fe and R subsystems when solving the self-consistent problems based on Hamiltonians (1) and (2) provided the corresponding thermodynamic potential is minimal (see Eqs. (8) and (9) in [10] and Eqs. (6) and (7) in [11]) in order to determine the stability regions of various magnetic phases, the phase transition fields, magnetization curves, the magnetic susceptibility, and so on.

4. RESULTS AND DISCUSSION

To find crystal field parameters B_q^k, we used experimental data for the temperature dependences of initial magnetic susceptibility $\chi_{c,\perp c}(T)$ and magnetization curves $M_{c,\perp c}(B)$ at $T = 2$ K. Based on the criterion of the best description of characteristics $\chi_{c,\perp c}(T)$ and $M_{c,\perp c}(B)$, the well-known splittings of the ground multiplet of the Sm^{3+} ion, and Δ_{fd} from [5], we chose the following set of crystal field parameters B_q^k: $B_0^2 = 285$ cm^{-1}, $B_0^4 = -900$ cm^{-1}, and $B_3^4 = -1520$ cm^{-1}. This set of B_q^k corresponds to the spectroscopic characteristics of the Sm^{3+} ion given in the table. The calculated energies of the ground multiplet of the Sm^{3+} ion coincide with those found in [5]. The components of the g tensor of the ground doublet of the Sm^{3+} ion ($g_c = 0.36$, $g_a = 0.53$) do not contradict the corresponding values taken in [7] ($g_c \approx 0.3$, $g_\perp \approx 0.3$). Our components of the g tensor indicate that the Sm subsystem at low temperatures weakly stabilizes the easy-plane state. When the f–d interaction is taken into account at $T < T_N$, the degeneracy of the Kramers doublets is removed and the low-temperature splitting of the ground doublet ($\Delta_{\mathrm{fd}} = 13.2$ cm^{-1}) at $\lambda_{\mathrm{fd}}^{\mathrm{Sm}} = -3.53$ T/μ_B coincides with Δ_{fd} known from [5].

The magnetic characteristics presented in the next figures are calculated for the parameters from the table, which also gives the well-known reported data and (for comparison) the parameters of easy-plane $NdFe_3(BO_3)_4$ [11]. In the calculations, we also used the following anisotropy constants of the Fe subsystem: $K_2^{\mathrm{Fe}} = 0.48$ T μ_B and $K_6^{\mathrm{Fe}} = -7.5 \times 10^{-3}$ T μ_B (see Eq. (8) in [11]).

The high field of the f–d interaction ($B_{fd}^{\mathrm{Sm}} = 53$ T) as compared to the ferroborates studied to date (see the tables in [12, 14]) is caused by the large splitting of the ground doublet of the Sm^{3+} ion ($\Delta_{\mathrm{fd}} = 13.2$ cm^{-1}) experimentally determined in [5] at a low value of g tensor component g_a, the smallness of which is also related to the Landé factor $g_J^{\mathrm{Sm}} = 2/7$,

$$\Delta_{fd} = \mu_B g_a B_{fd}^{\mathrm{Sm}}.$$

Note that the critical field in which the sign of electric polarization and magnetostriction in $SmFe_3(BO_3)_4$ changes (according to [2], it corresponds to the f–d exchange field) was estimated in [6] from the corresponding field for $NdFe_3(BO_3)_4$, which is 5 T [2]. This field is estimated to be 30 T, which is lower than the value determined from the well-known splitting of the fundamental doublet at $g_a = 0.53$ (or $g_\perp \approx 0.3$ from [7]; see table). Note also that the calculated magnetic moment of the Sm sublattice at $T = 2$ K and $B = 0$ is $m_i^{\mathrm{Sm}} \approx 0.32\mu_B$, which is slightly higher than the value ($0.24\mu_B$) given in [19].

Figure 1 shows the experimental magnetization curves $M_{c,\perp c}(B)$ for $SmFe_3(BO_3)_4$ in the basal plane (a) and along the c axis (b) at $T = 2$, 30, and 300 K. It is seen that the $M_{c,\perp c}(B)$ curves change with temperature, which is caused by a decrease in the magnetic moments of the Fe and Sm subsystems. The magnetization curves of $SmFe_3(BO_3)_4$ in the basal plane at $B > 1.5$ T and along the trigonal axis change weakly, which indicates the same character of magnetization. The magnetic moments of the Fe subsystem bend toward the field, exhibiting perpendicular susceptibility, and

Parameters of $SmFe_3(BO_3)_4$ and $NdFe_3(BO_3)_4$ [11]

Compound	$SmFe_3(BO_3)_4$		$NdFe_3(BO_3)_4$
$B_{dd1} = \lambda_1 M_0$, T	64 [6]*	59	58
λ_1, T/μ_B	−4.27 [6]*	−3.93	−3.87
$B_{fd}^R = \lambda_{fd}^R M_0$, T	30 [6], 35 [8] 94**	53	7.1
λ_{fd}^R, T/μ_B		−3.53	−0.47
$\Delta_{fd} = \mu_B g_a \lvert\lambda_{fd}^{Sm}\rvert M_0$, cm^{-1}	13.2 [5]	13.2 ($T = 2$ K)	8.8 ($T = 2$ K)
$\Delta = E_i - E_1$ ($i = 1$–6), cm^{-1}, ($B = 0$)	0, 135, 220 [5]	0, 135, 220 ($T > T_N$)	0, 65, 140 ($T > T_N$)
		0, 13.2, 141.8, 141.9, 225, 233 ($T = 2$ K)	0, 8.8, 69, 69, 140, 148 ($T = 2$ K)
$g_{\perp c}$	~0.3 [7]	~0.53	2.6
g_c	~0.3 [7]	~0.36	1.0

Notes: B_{dd1} and B_{fd} are the low-temperature exchange fields corresponding to molecular constants λ_1 and B_{fd}^R, respectively; Δ_{fd} is the low-temperature splitting of the fundamental doublet of the Sm^{3+} or Nd^{3+} ion induced by the f–d interaction; Δ is the low-level energy of the fundamental doublet of the Sm^{3+} or Nd^{3+} ion; $g_{\perp c}$ and g_c are the g tensor components of the fundamental doublet of the Sm^{3+} or Nd^{3+} ion; and $M_0 = |M_i(T = 0, B = 0)| = 15\mu_B$ is the magnetic moment of Fe per formula unit.

* The parameter was estimated from the quantity $\chi_\perp^{Fe} = 0.12 \times 10^{-3}$ cm^3/g (at $H \approx 10$ kOe) given in [6].

** The parameter was estimated by the formula $B_{fd} = \lvert\lambda_{fd}^{Sm}\rvert M_0 = \Delta_{fd}/\mu_B g_\perp$ at $\Delta_{fd} = 13.2$ cm^{-1} [5] and $g_\perp \approx 0.3$ [7].

the Sm subsystem demonstrates an increase in the magnetic field component along the field (see the diagrams in Fig. 2). It is also seen from Fig. 1 that the calculated magnetization curves $M_{c,\perp c}(B)$ in the paramagnetic region at $T = 300$ K well describe the experimental data. It is seen from the inset to Fig. 1 that the magnetic susceptibility in the paramagnetic phase is almost isotropic and that it becomes anisotropic at $T < T_N$: $\chi_{\perp c}(T)$ decreases sharply in the basal plane as compared to $\chi_{\perp c}(T)$, which changes much weaker. A similar character of magnetization curves measured at $T \leq 110$ K was detected in [6]. It is this behavior of magnetic susceptibility that would be expected for the antiferromagnetic ordering in the Fe subsystem, which makes the main contribution to the susceptibility.

A low but noticeable anisotropy is seen from the experimental $M_{c,\perp c}(B)$ curves at $T = 2$ K shown in Fig. 2. The anisotropy detected experimentally cannot be reproduced when only the parameters given above are taken into account. The calculations performed on the assumption of a misoriented field demonstrate that, for better agreement with the experimental results, the angle of field misorientation should be 6°–8°, which is unlikely. Only when the anisotropic Sm–Fe exchange interaction was taken into account, we were able to describe the experimental results rather accurately (Fig. 2). The Hamiltonian of the anisotropic Sm–Fe exchange interaction was taken in the form proposed in [20] (see Eq. (8)). To achieve agreement, we chose two parameters $a_0^2 = 13$ cm^{-1} and $a_0^4 = -15$ cm^{-1} (in the designations of [20]), which are comparable with the values of $a_0^{2,4}$ for $PrFe_3(BO_3)_4$ [20]. Note that it is sufficient to take into account only the anisotropic part of the R–Fe exchange interaction for the large volumes of the experimental data for the magnetic, magnetoelastic, and spectroscopic characteristics of rare-earth ferroborates with R = Pr, Nd, Tb, Dy, Ho, and Er to be sucessfuly described using the given approach [10–15].

We now consider the low-field region of the experimental magnetization curve $M_{\perp c}(B)$ at $T = 2$ K, where the initial segment is nonlinear, in more detail. If the $M_{\perp c}(B)$ curve is differentiated, a pronounced peak near 1 T is revealed. Three types of domains are possible in the case of a trigonal crystal with magnetic moments lying in the basal plane. During magnetization in the basal plane in low fields, all three domains with antiferromagnetism axes making an angle of 120° with each other contribute to the magnetization (see the schematic diagram at the top of Fig. 3). The $M_{\perp c}(B)$ curves at $B < 1.5$ T were calculated using the

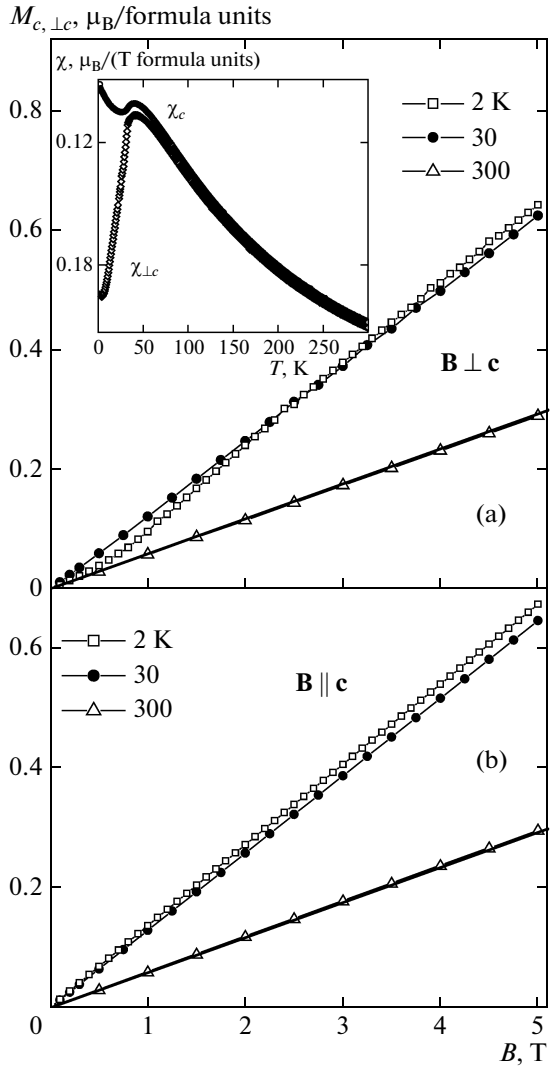

Fig. 1. Experimental magnetization curves of $SmFe_3(BO_3)_4$ for (a) $\mathbf{B} \perp \mathbf{c}$ and (b) $\mathbf{B} \parallel \mathbf{c}$ at $T = 2$, 30, and 300 K: (solid lines) magnetization curves calculated at $T =$ 300 K. (inset) Temperature dependences of initial magnetic susceptibility $\chi_{c,\perp c}(T)$ measured at $B = 0.1$ T.

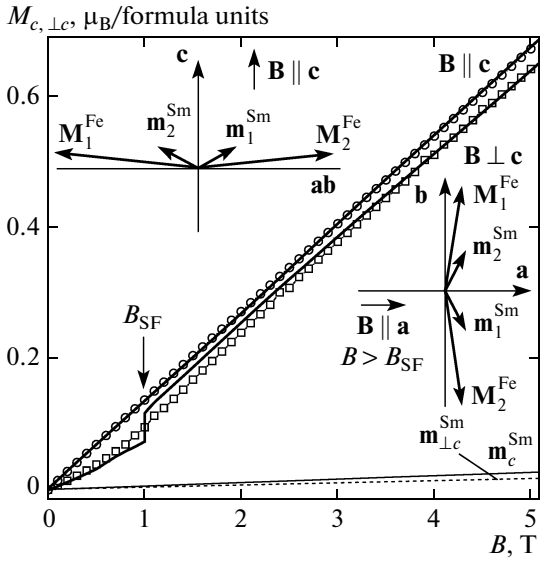

Fig. 2. Magnetization curves of $SmFe_3(BO_3)_4$ for $\mathbf{B} \parallel \mathbf{c}$ and $\mathbf{B} \perp \mathbf{c}$ at $T = 2$ K: (symbols) experimental data and (lines) calculation. (inset) Schemes of the orientations of magnetic moments $\mathbf{M}_i^{Fe}$ and $\mathbf{m}_i^{Sm}$ used to calculate the magnetization in the flop phase. $m_{c,\perp c}^{Sm}$ is the calculated contribution of the Sm subsystem to the magnetization at (solid line) $\mathbf{B} \parallel \mathbf{c}$ and (dashed line) $\mathbf{B} \perp \mathbf{c}$.

approach suggested in [11], where the magnetization processes in easy-plane $NdFe_3(BO_3)_4$ were comprehensively studied with allowance for the possible existence of all three types of domains.

Our calculations show that magnetization processes are different at different directions of a field in the basal plane: at $\mathbf{B} \parallel \mathbf{a}$, this is a spin-flop transition in a domain with an antiferromagnetism axis along axis **a**; at $\mathbf{B} \parallel \mathbf{b}$, this is the breakaway of 30° domains in a certain critical field. When **B** has any other direction, this is breakaway in a domain with the minimum angle between its easy axis and the field. Our calculations demonstrate that the spin-flop transition field for $\mathbf{B} \parallel \mathbf{a}$ and the breakaway fields in domains for other field directions differ weakly and that the calculated magnetization curves are very similar. Thus, the situation is analogous to the case of $NdFe_3(BO_3)_4$ [11]. It is important that the entire sample transforms into a flop phase jumpwise at a certain field directed in the basal plane. We take into account a similar character of the magnetization curves for different field directions in the basal plane and, for simplicity, compare the case $\mathbf{B} \parallel \mathbf{a}$ with the experimental data.

At $\mathbf{B} \parallel \mathbf{a}$, the magnetic moments of iron in a domain with an antiferromagnetism axis directed along the field do not contribute to the magnetization at $T = 2$ K (dashed vectors $\mathbf{M}_{1,2(0)}^{Fe}$ at the top of Fig. 3). In the Sm subsystem, $\mathbf{m}_1^{Sm}$ directed opposite to the field decreases. As a result, the total magnetization of this domain increases weakly with the field. In two other domains with antiferromagnetism axes directed at an angle of 60° to the field (which are equivalent with respect to direction $\mathbf{B} \parallel \mathbf{a}$), both magnetic moments of iron $\mathbf{M}_{1,2(60)}^{Fe}$ in each domain rotate toward the flop state. It is seen from the calculated field dependence of the angle of rotation of vectors $\mathbf{M}_{1,2(60)}^{Fe}$ in the *ab* plane (Fig. 3) that vector $\mathbf{M}_{1(60)}^{Fe}$ rotates slightly faster than vector $\mathbf{M}_{2(60)}^{Fe}$. Due to the different rates of rotation, the contribution of these domains increases. The total

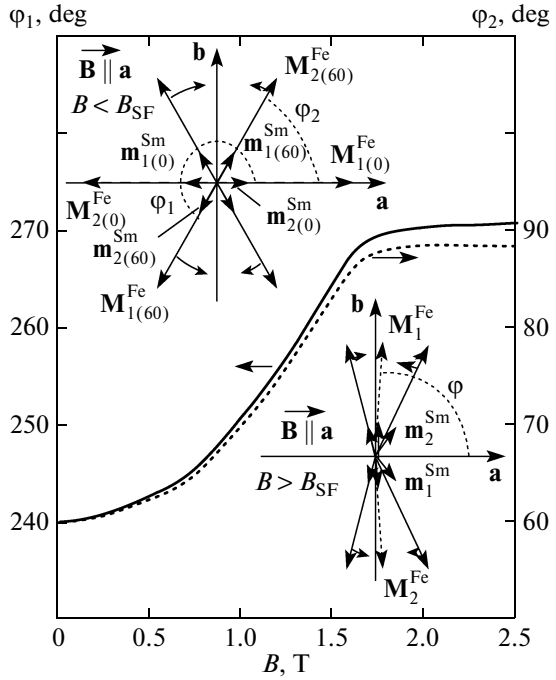

Fig. 3. Calculated field dependence of the angle of deviation of magnetic moments $\mathbf{M}^{\mathrm{Fe}}_{1,2(60)}$ from axis a in the ab plane: $\varphi_1 = 240°$ at $B = 0$ for $\mathbf{M}^{\mathrm{Fe}}_{1(60)}$ and $\varphi_2 = 60°$ at $B = 0$ for $\mathbf{M}^{\mathrm{Fe}}_{2(60)}$. (insets) Schemes of the orientations of $\mathbf{M}^{\mathrm{Fe}}_i$ and $\mathbf{m}^{\mathrm{Sm}}_i$ used to calculate the magnetization before ($B < B_{\mathrm{SF}}$) and after ($B > B_{\mathrm{SF}}$) the spin-flop transition at $\mathbf{B} \parallel \mathbf{a}$ (axis c is normal to the figure plane). Different lengths of the arrows indicating the direction of $\mathbf{M}^{\mathrm{Fe}}_{1,2(60)}$ rotation correspond to different rates of rotation.

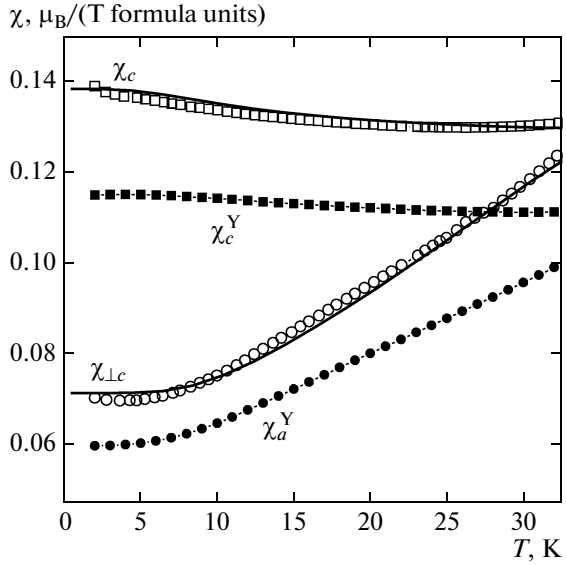

Fig. 4. Temperature dependences of the initial magnetic susceptibility of (open symbols) $SmFe_3(BO_3)_4$ ($\chi_{c,\perp c}(T)$) and (solid symbols) $YFe_3(BO_3)_4$ ($\chi^{\mathrm{Y}}_{a,c}(T)$) [21] at $B = 0.1$ T. (symbols) Experimental data and (lines) calculation.

magnetization for field $\mathbf{B} \parallel \mathbf{a}$ and $B < 1$ T is

$$M_a = \frac{1}{2}\left[\frac{1}{3}(M^{\mathrm{Fe}}_0 + m^{\mathrm{Sm}}_{1(0)a} + m^{\mathrm{Sm}}_{2(0)a}) + \frac{2}{3}(M^{\mathrm{Fe}}_{60} + m^{\mathrm{Sm}}_{1(60)a} + m^{\mathrm{Sm}}_{2(60)a})\right] \quad (5)$$

and well describes the experimental $M_{\perp c}(B)$ curve (see Fig. 2). In Eq. (5), $M^{\mathrm{Fe}}_0 = M^{\mathrm{Fe}}_{1(0)} - M^{\mathrm{Fe}}_{2(0)}$ and $M^{\mathrm{Fe}}_{60} = M^{\mathrm{Fe}}_{1(60)}\cos\varphi_1 + M^{\mathrm{Fe}}_{2(60)}\cos\varphi_2$ are the contributions of iron to the magnetization of the compound with allowance for the projection onto axis a. In a field $B_{\mathrm{SF}} \approx 1$ T, a spin-flop transition into the state with magnetic moments that are almost perpendicular to the field occurs in a domain with the magnetic moment of the Fe subsystem directed along axis a, and the contribution to the magnetization is now $M^{\mathrm{Fe}}_{\mathrm{flop}} = 2M^{\mathrm{Fe}}_1\cos\varphi$ (see the schematic diagram at the bottom of Fig. 3). As a result, the magnetization of the compound at $B > B_{\mathrm{SF}}$ is determined by Eq. (5) upon the substitution of M^{Fe}_0 for $M^{\mathrm{Fe}}_{\mathrm{flop}}$.

When field $\mathbf{B} \parallel \mathbf{a}$ increases further, the rotation of $\mathbf{M}^{\mathrm{Fe}}_{1,2(60)}$ continues and, beginning from fields of about 1.5 T, the resulting magnetization is determined by approximately the same contribution from all domains, which corresponds to the flop phase of the entire sample (see Figs. 2, 3). Note that the rotations and jumps of the magnetic moments of Fe in domains are accompanied by the corresponding changes in the components of the magnetic moments of the Sm subsystem.

Figure 4 shows the low-temperature regions (at $T < T_{\mathrm{N}}$) of the experimental and calculated dependences of the magnetic susceptibility $\chi_{c,\perp c}(T)$. It is seen that susceptibility $\chi_{c,\perp c}(T)$ of $SmFe_3(BO_3)_4$ differs weakly from the susceptibility of $YFe_3(BO_3)_4$ [21], which indicates a low contribution from the Sm subsystem. During magnetization in the basal plane for $B = 0.1$ T, the contribution to susceptibility $\chi_{c,\perp c}(T)$ is made by all possible domains, and the magnetization of $SmFe_3(BO_3)_4$ proceeds similarly to the magnetization processes described above in calculating magnetization M_a (Eq. (5)). For a field directed along axis c, the sample is in the flop phase and behaves like a single-domain sample (see the diagram at the top of Fig. 2). The weak decrease in the $\chi_{\perp c}(T)$ with increasing temperature is related to a decrease in the contribution of paramagnetic ion Sm^{3+} against the background of a constant perpendicular susceptibility of the antiferromagnetic Fe subsystem.

5. CONCLUSIONS

The magnetic properties of $SmFe_3(BO_3)_4$ were studied experimentally and theoretically, and agreement between the experimental and calculated data was obtained for the entire set of measured characteristics. The actual parameters of $SmFe_3(BO_3)_4$ are determined during a comparison of the experimental and calculated results.

The anisotropy of the $M_{c,\perp c}(B)$ curves detected experimentally was shown to be well described if the anisotropy of the Sm–Fe exchange interaction is taken into account. During magnetization along axis a in a field of about 1 T, a spin-flop transition in one of the three possible domains resulting from trigonal symmetry causes the shape of the $M_{\perp c}(B)$ curves that is characteristic of a first-order phase transition diffused under real domain structure conditions. A correct calculation of the magnetization processes in weak fields led to a description of the temperature dependences $\chi_{c,\perp c}(T)$ at $T < T_N$. $SmFe_3(BO_3)_4$ should be studied further, since the magnetic and other properties of $SmFe_3(BO_3)_4$ can be substantially affected by mixing of the multiplets of the Sm^{3+} ion (J–J coupling), by analogy with $Sm_3Fe_5O_{12}$ [22].

ACKNOWLEDGMENTS

This work was supported by the Russian Foundation for Basic Research, project no. 12-02-31007mol_a.

REFERENCES

1. A. K. Zvezdin, S. S. Krotov, A. M. Kadomtseva, G. P. Vorob'ev, Yu. F. Popov, A. P. Pyatakov, L. N. Bezmaternykh, and E. A. Popova JETP Lett. **81** (6), 272 (2005).
2. A. K. Zvezdin, G. P. Vorob'ev, A. M. Kadomtseva, Yu. F. Popov, A. P. Pyatakov, L. N. Bezmaternykh, A. V. Kuvardin, and E. A. Popova JETP Lett. **83** (11), 509 (2006).
3. A. M. Kadomtseva, Yu. F. Popov, G. P. Vorob'ev, A. P. Pyatakov, S. S. Krotov, K. I. Kamilov, V. Yu. Ivanov, A. A. Mukhin, A. K. Zvezdin, A. M. Kuz'menko, L. N. Bezmaternykh, I. A. Gudim, and V. L. Temerov, Low Temp. Phys. **36** (6), 511 (2010).
4. A. A. Mukhin, G. P. Vorob'ev, V. Yu. Ivanov, A. M. Kadomtseva, A. S. Narizhnaya, A. M. Kuz'menko, Yu. F. Popov, L. N. Bezmaternykh, and I. A. Gudim, JETP Lett. **93** (5), 275 (2011).
5. E. P. Chukalina, M. N. Popova, L. N. Bezmaternykh, and I. A. Gudim, Phys. Lett. A **374**, 1790 (2010).
6. Yu. F. Popov, A. P. Pyatakov, A. M. Kadomtseva, G. P. Vorob'ev, A. K. Zvezdin, A. A. Mukhin, V. Yu. Ivanov, and I. A. Gudim JETP **111** (2), 199 (2010).
7. A. M. Kuz'menko, A. A. Mukhin, V. Yu. Ivanov, A. M. Kadomtseva, and L. N. Bezmaternykh, JETP Lett. **94** (4), 294 (2011).
8. A. M. Kadomtseva, G. P. Vorob'ev, Yu. F. Popov, A. P. Pyatakov, A. A. Mukhin, V. Yu. Ivanov, A. K. Zvezdin, I. A. Gudim, V. L. Temerov, and L. N. Bezmaternykh, JETP **114** (5), 810 (2012).
9. I. A. Gudim, E. V. Eremin, and V. L. Temerov, J. Cryst. Growth **312**, 2427 (2010).
10. E. A. Popova, D. V. Volkov, A. N. Vasiliev, A. A. Demidov, N. P. Kolmakova, I. A. Gudim, L. N. Bezmaternykh, N. Tristan, Yu. Skourski, B. Büchner, C. Hess, and R. Klingeler, Phys. Rev. B: Condens. Matter **75**, 224413 (2007).
11. D. V. Volkov, A. A. Demidov, and N. P. Kolmakova, JETP **104** (6), 897 (2007).
12. D. V. Volkov, A. A. Demidov, and N. P. Kolmakova, JETP **106** (4), 723 (2008).
13. A. A. Demidov, N. P. Kolmakova, D. V. Volkov, and A. N. Vasiliev, Physica B: Condens. Matter **404**, 213 (2009).
14. A. A. Demidov and D. V. Volkov, Phys. Solid State **53** (5), 985 (2011).
15. A. A. Demidov and D. V. Volkov, Phys. Solid State **54** (3), 537 (2012).
16. Y. Hinatsu, Y. Doi, K. Ito, M. Wakeshima, and A. Alemi, J. Solid State Chem. **172**, 438 (2003).
17. S. A. Al'tshuler and B. M. Kozyrev, *Electron Paramagnetic Resonance in Compounds of Transition Elements* (Nauka, Moscow, 1972; Israel Program for Scientific Translations, Jerusalem, 1975).
18. A. K. Zvezdin, V. M. Matveev, A. A. Mukhin, and A. I. Popov, *Rare-Earth Ions in Magnetically Ordered Crystals* (Nauka, Moscow, 1985) [in Russian].
19. C. Ritter, A. Pankrats, I. Gudim, and A. Vorotynov, in *Abstracts of Papers of the 19th International Conference on Magnetism with Strongly Correlated Election Systems, Busan Exhibition and Convention Center (BEXCO), Busan, Korea, July 8–13, 2012* (Busan, 2012), p. 97.
20. M. N. Popova, T. N. Stanislavchuk, B. Z. Malkin, and L. N. Bezmaternykh, Phys. Rev. B: Condens. Matter **80**, 195101 (2009).
21. E. A. Popova, A. N. Vasiliev, V. L. Temerov, L. N. Bezmaternykh, N. Tristan, R. Klingeler, and B. Büchner, J. Phys.: Condens. Matter **22**, 116006 (2010).
22. O. A. Dorofeev and A. I. Popov, Sov. Phys. Solid State **32** (11), 1983 (1990).

Translated by K. Shakhlevich